JOURNAL OF MATERIALS SCIENCE **40** (2005) 3601 – 3605

# Characterization of FGM monomorph actuators fabricated using EPD

T. LI*, Y. H. CHEN, J. MA
*Ceramics Lab, School of Materials Science and Engineering, Nanyang Technological University, Singapore 639798*
*E-mail: tli@ntu.edu.sg*

Piezoelectric FGM monomorph actuators fabricated using electrophoretic deposition (EPD) were investigated. Both the physical and electromechanical properties were examined. The high voltage performance of the actuator in both static and dynamic state was focused. It was found that the monomorph exhibits tetragonal phase perovskite structure and the gradient variation of microstructure was observed over the cross section. The displacement keeps a wide range of linearity in the static state. In the dynamic state, the vibration displacement is both frequency and voltage dependent. The resonant frequency shifts to lower frequency range due to the higher vibration loss at higher voltages. This results in the frequency dependence of the vibration limitations. The vibration limitation is also voltage dependent. Above a cutoff voltage, the displacement may not increase. To obtain a higher resonant displacement or velocity, the frequency and voltage should match well. Temperature rise or heat generation is caused by vibration loss. The maximum temperature happens at the clamped end of the monomorph.


## 1. Introduction

Piezoelectric bimorph and unimorph actuators are important for bending actuations. They are able to produce a relative large displacement compared with the piezo stack or multilayer actuators [1]. Application of the bimorph actuator covers a wide range, including positioners, microphones, piezo pumps and ultrasonic motors. However, the bimorph or unimorph actuator is usually fabricated by bonding piezoelectric plates with elastic layers. This reduces the reliability, limits the performance and discourages applications of the actuators because the actuator may delaminate at the contact bonding surface [2].

To avoid or minimize such a problem, actuators without bonding layers, called monomorph, has been proposed and developed. One such actuator is the functional gradient materials (FGM) monomorph fabricated using electrophoretic deposition (EPD) [3–6]. This actuator exhibits compositional, microstructural and functional gradient over the cross section. A goodness of this configuration is the smooth stress distribution, which is supposed to be able to increase the reliability and life span of the actuator. The actuator was fabricated by depositing different compositional layers on the substrate and then cosintering. An important feature of EPD is that a miniaturized actuator can be fabricated.

The fabrication, modeling and parts of the work on characterization of the monomorph actuator have been introduced in the papers published earlier [3–6]. However, the work mainly focused on the static and low voltage situations. In this paper, a more complete study was carried out. The purpose is to investigate the performance of the actuator both at static and dynamic state. The high voltage range properties were focused. The physical properties were also examined.

## 2. Experimental

Two starting piezoelectric materials $Pb(Zr_{0.52}Ti_{0.48})O_3$ (PZT0) and $0.95Pb(Zr_{0.52}Ti_{0.48})O_3{\cdot}0.03BiFeO_3{\cdot}0.02Ba(Cu_{0.5}W_{0.5})O_3$+0.5 wt%$MnO_2$(PZT1) prepared using the conventional oxide mixing technique were applied to fabricate the monomorph actuator. Six suspensions with composition $x\text{PZT1} + (1-x)\text{PZT0}$ $(x = 0.1 - 0.6)$ were prepared. The powder concentration was 50 kg/m$^3$ and the suspension pH was controlled to be 4.6. The suspension was stirred for 3 to 6 h to make sure the complete dissolution and dispersion of the powders in the medium. Then six suspensions were deposited on the substrate consecutively. After drying, the deposition was sintered at 1100°C for 1 h. Finally, the sintered product was cut into the rectangular shape, coated with silver electrode and poled in silicone oil at 100°C for 30 min under 2 kV/mm.

The physical properties, phase and microstructure, were examined using XRD (Rigaku dmax2200, Cu $K_\alpha$

*Author to whom all correspondence should be addressed.

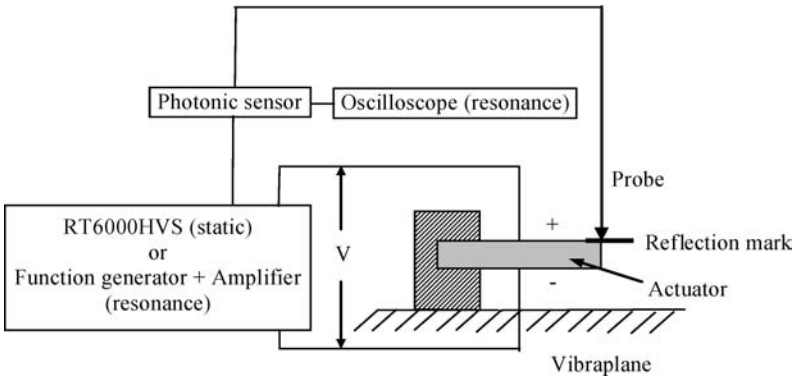


*Figure 1* Characterization setup of the monomorph actuator.

radiation, $\lambda = 0.154$ nm) and SEM (Jeol JSM 5410LV), respectively. The electromechanical properties, static and dynamic bending displacement, were measured using the setup as shown in Fig. 1. It consists of RT6000HVS ferroelectric tester (Radiant Technologies, Inc.), Vibraplane (RS Kinetic Systems, Inc.), MTI-2000 photonic sensor (probe: MTI2032RX, MTI Instruments), FG3000 function generator (Yokogawa), PZD2000 high voltage amplifier (Trek) and DL1640L oscilloscope (Yokogawa). The sample to be measured was clamped to the vibraplane at one end and free at the other end. The photonic sensor was used to measure the displacement. RT6000HVS ferroelectric tester was utilized for static displacement measurement. A triangle signal was generated and applied to the sample by the tester. The measurement frequency is 2.5 Hz. The displacement data from the photonic sensor were recorded by the tester. In the dynamic measurement, the ferroelectric tester was replaced with the function generator, high voltage amplifier and oscilloscope. Function generator and voltage amplifier are the driving system and provide sinusoidal signal. The displacement data were read from the oscilloscope. Finally, the temperature distribution was measured using IRISYS thermal imager (Charslton Technologies Pte Ltd).

## 3. Results and discussions

### 3.1. Phase and microstructure

Fig. 2 illustrates the X-ray diffraction patterns of the sintered monomorph. The tetragonal phase of perovskite structures can be identified from the figure. This is the usual phase structure of the PZT materials. Fig. 3 shows the microstructure of the monomorph. A gradient variation of the grain size can be observed from the left to the right side of the cross section. The compositional and microstructural gradient induced variation in piezoelectric properties over the cross section is the driving source of the monomorph actuator.

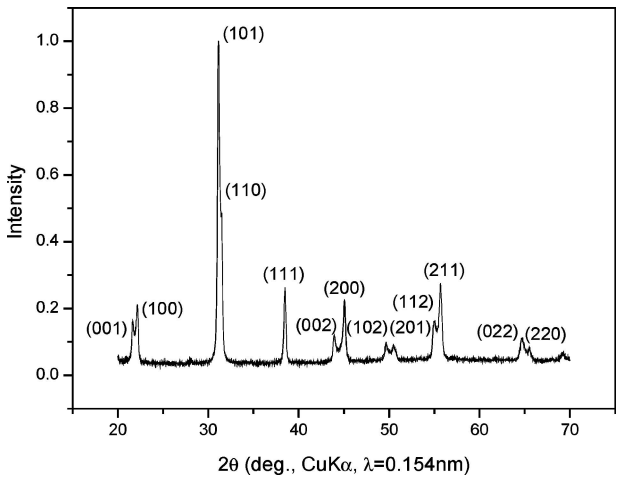


*Figure 2* XRD patterns of the monomorph actuator.

### 3.2. Static bending displacement

The static displacement was measured from low voltage to high voltage using a sample with a dimension 15.97 mm in length, 2.94 mm in width and 0.37 mm in thickness (15.97-2.94-0.37). Fig. 4b illustrates the displacement-voltage hysteresis loop. It can be seen that the displacement remains linear in a wide range from 0 to 1000 V (2.7 kV/mm). However, as the voltage increases, the hysteresis becomes large indicating the higher loss at higher voltages. The loss is the result of domain wall motion and domain switching [7]. Fig. 4a shows the maximum displacement obtained in each hysteresis loop at the respective set voltage in Fig. 4b. The displacement increases linearly and monotonically. At 1000 V, a displacement of 16.69 $\mu$m has been achieved.

### 3.3. Resonant displacement and velocity

The displacement near the resonant frequency was measured at different voltages as shown in Fig. 5b. As the voltage increases, the displacement increases accordingly in the measurement range. However, the resonant frequency shifts to the lower voltage side. This is due to the increase of the losses at higher voltages as discussed earlier.

The root-mean-square (rms) vibration velocity at the free end of the actuator was also measured as shown in Fig. 5a. Rms vibration velocity is a universal parameter, which measures the motional speed of the actuator. High power applications such as ultrasonic motor and piezoelectric fans, prefer a high vibration velocity to obtain high performance of the device. The rms vibration velocity is a function of both displacement and excitation frequency. Under harmonic excitation, the instantaneous displacement $u$ of the actuator can be

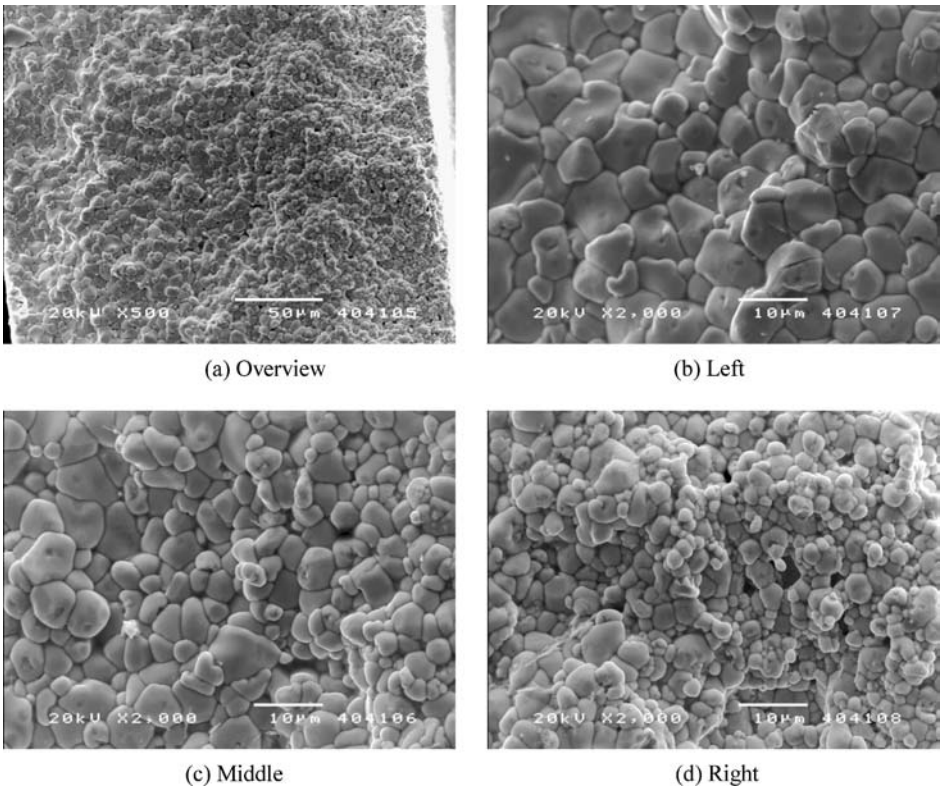


*Figure 3* Microstructure of the monomorph actuator.

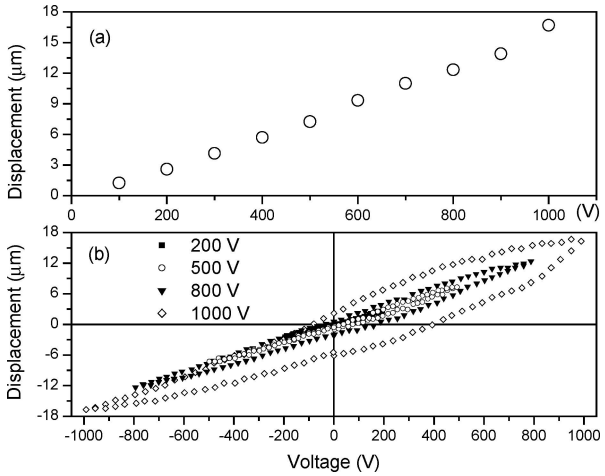


*Figure 4* Static displacement of the monomorph actuator 15.97-2.94-0.37.

expressed as:

$$u = U \sin(\omega t) \tag{1}$$

where $U$ is the vibration amplitude, $\omega$ is the frequency and $t$ is the time. The instantaneous velocity of the actuator is the derivative of the displacement:

$$v = \mathrm{d}u/\mathrm{d}t = \omega U \cos(\omega t) \tag{2}$$

The rms vibration velocity in a cycle $T$ can then be obtained as:

$$v_{rms} = \sqrt{1/T \int_0^T v^2 \mathrm{d}t} = \omega U/\sqrt{2} \tag{3}$$

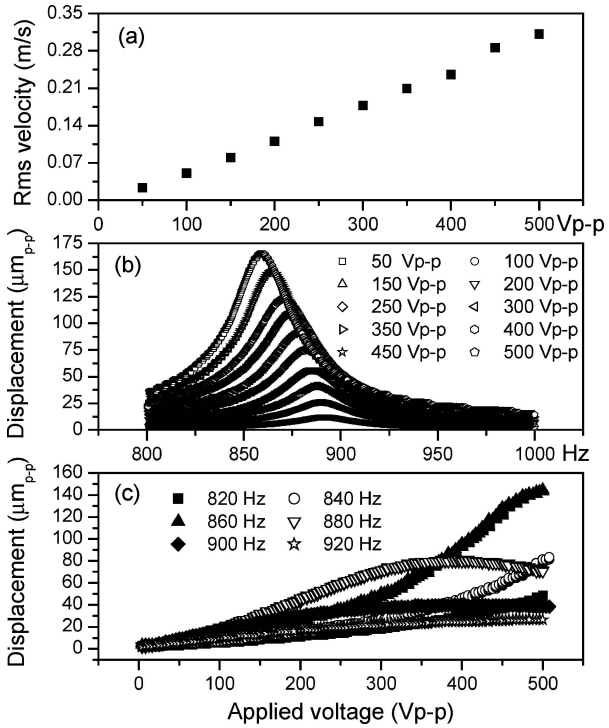


*Figure 5* Dynamic displacement and rms vibration velocity of the monomorph actuator 15.97-2.94-0.37.

The rms vibration velocity, resonance frequency and vibration amplitude as a function of applied voltage have been listed in Table I. Fig. 5a and Table I show that the velocity increases linearly in the studied range. The rms vibration velocity 0.31 m/s has been achieved at 500 $V_{p-p}$.

Fig. 5c is the voltage scan of the displacement. The voltage increases linearly from 0 to 500 $V_{p-p}$. The

TABLE I Resonant frequency, vibration amplitude and rms vibration velocity of the monomorph actuator 15.97-2.94-0.37

| Applied voltage ($V_{p-p}$) | Resonant frequency (Hz) | Vibration amplitude ($\mu m_{p-p}$) | Rms velocity (m/s) |
|---|---|---|---|
| 50 | 892 | 12 | 0.02 |
| 100 | 892 | 26 | 0.05 |
| 150 | 890 | 41 | 0.08 |
| 200 | 887 | 57 | 0.11 |
| 250 | 883 | 76 | 0.15 |
| 300 | 881 | 92 | 0.18 |
| 350 | 876 | 109 | 0.21 |
| 400 | 872 | 123 | 0.24 |
| 450 | 865 | 150 | 0.29 |
| 500 | 860 | 165 | 0.31 |

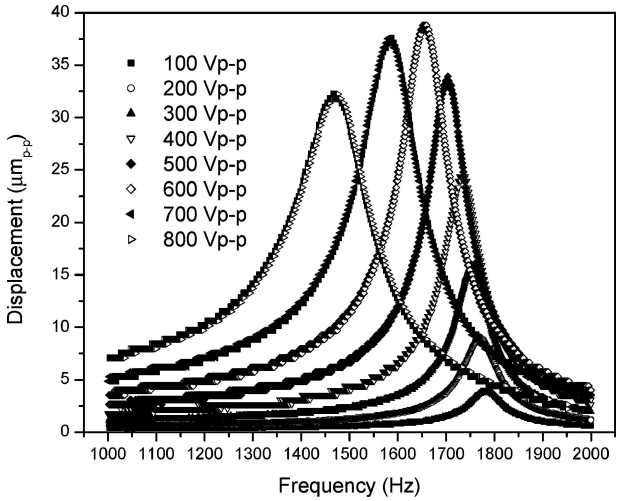


*Figure 6* Vibration limitation of the monomorph actuator 9.44-2.88-0.45.

measurement was performed at different fixed frequencies. It can be seen that both the slope and maximum value of the displacements curve at different frequencies are largely different. This can be explained using Fig. 5b. At a higher frequency above the resonance (no loss natural frequency), such as 920 Hz, the displacement cannot achieve a large value even a high voltage is applied due to the fact that there exists no resonance. However, at a lower frequency, such as 880 Hz, much larger displacement can be achieved. This is due to the reason that 880 Hz is roughly the resonance of 300 $V_{p-p}$ as seen in Fig. 5b. Above 300 $V_{p-p}$, the displacement may still increase a little as seen in Fig. 5c. But, too high a voltage may drop the displacement at this frequency due to the shift of the resonance at higher voltages as mentioned earlier. However, also due to this shift, an even higher displacement can be achieved at a lower frequency, for example 860 Hz. Further reducing the frequency, to reach a large displacement, a higher voltage may be required. So the displacement at 820 Hz is not large because that 500 $V_{p-p}$ is not enough to excite resonance at this frequency. The above analysis shows that displacement is both frequency and voltage dependent. In the frequency above the resonance (natural frequency), a large displacement cannot be achieved. While, in a certain range lower than the resonance, a large displacement can be achieved by increasing the voltage and reducing the frequency simultaneously. So, the frequency and voltage should match well to obtain the large displacement.

## 3.4. Vibration limitation

For high power application, it is essential to identify the vibration limitation of the actuators. In the static case, the limitation has been widely accepted as the coercive field of the actuator. However, in the dynamic resonance state, the answer is not such clear so far. Several effects, including mechanical strength, magnitude of electric field, temperature rise, crack generation, breakdown or burnout, may affect the results [8–15]. To find the vibration limitation, the displacement of a monomorph (9.44-2.88-0.45) as a function of frequency and voltage near the resonance was measured. The obtained result has been shown in Fig. 6. It is observed that there is a cutoff voltage of 600 $V_{p-p}$ where the maximum displacement was found. Below 600 $V_{p-p}$, the vibration displacement increases with the voltage. In contrast, above 600 $V_{p-p}$, the displacement never increases but decreases with the applied voltage. The reason may be the higher losses at the higher voltages as mentioned earlier. From this result, also considering Fig. 5c, it

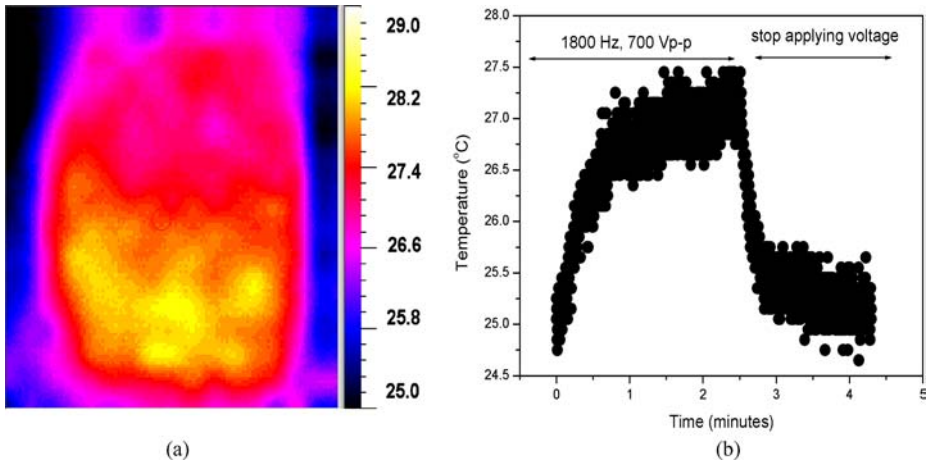


*Figure 7* Temperature rise and distribution of the monomorph actuator 10.72-2.56-0.37.

can be concluded that that the vibration limitation is both frequency and voltage dependant.

### 3.5. Temperature distribution

The temperature distribution of a monomorph (10.72-2.56-0.37) at the resonance condition was also observed. The temperature rise or heat generation is caused by the mechanical vibration losses [9–12]. As a result, parts of the input power won't convert to mechanical vibration but dissipates as heat [9, 10]. The maximum temperature was observed near the position of the fixed end as shown in Fig. 7a. It is consistent with the position of maximum stress, due to the fact that the vibration loss is proportional to the square of mechanical stress [11]. The maximum temperature rise is around 5°C. It saturates within 2 min as shown in Fig. 7b. The monomorph has a thin structure with high surface area (dissipate heat) to volume ratio (generate heat). This may help to prevent the heat generation or reduce the temperature rise. The monolithic structure may also be advantageous for reducing the vibration losses because the losses may still like to happen at the joints, connections and interfaces.

## 4. Conclusions

In this paper, the FGM monomorph fabricated using EPD was characterized. Important conclusions are:

(a) The fabricated monomorph shows perovskite structure with tetragonal phase. The gradient variation of microstructure due to the compositional gradient was observed over the cross section.

(b) The static displacement keeps a wide range of linearity (up to 1000 V in the studied case). However, the hysteresis becomes large at higher voltage due to higher losses.

(c) The vibration displacement near the resonant frequency is both frequency and voltage dependent. The resonant frequency shifts to lower frequency range at higher voltage. This results in the frequency dependence of the vibration limitations. At different frequencies, the obtained maximum displacement is different. The vibration limitation is also voltage dependent. There is a cutoff voltage. Above it, the displacement will not increase. The maximum displacement or vibration velocity can be obtained by lowering the frequency and meanwhile increasing the voltage in a certain frequency range. The frequency and voltage should match well.

(d) The maximum temperature happens at the maximum stress position (clamped end) of the monomorph actuator. The thin and monolithic structure of the monomorph may help to suppress heat generation.

## References


1. K. UCHINO, in "Piezoelectric Actuators and Ultrasonic Motors" (Kluwer Academic Publishers, Boston/Dordrecht/London, 1997) p. 130.
2. X. H. ZHU and Z. Y. MENG, *Sensor. Actuat.* **A48** (1995) 169.
3. Y. H. CHEN and J. MA, *Mater. Sci. Forum.* **437/438** (2003) 487.
4. Y. H. CHEN, T. LI and J. MA, *J. Mater. Sci.* **38** (2003) 2803.
5. Y. H. CHEN, J. MA and T. LI, *Ceram. Int.* **30** (2004) 1807.
6. *Idem.*, *ibid.* **30** (2004) 683.
7. B. K. MUKHERJEE and S. SHERRIT, in "Fifth International Congress on Sound and Vibration" (Adelaide, South Australia, 1997) p. 395.
8. T. KANDA, Y. KOBAYASHI and T. HIGUCHI, *Jpn. J. Appl. Phys.* **42** (2003) 3014.
9. S. TAKAHASHI, Y. SASAKI and K. UCHINO, *ibid.* **34** (1995) 5328.
10. M. UMEDA, K. NAKAMURA and S. UEHA, *ibid.* **38** (1999) 5581.
11. S. TASHIRO, M. IKEHIRO and H. IGARASHI, *ibid.* **36** (1997) 3004.
12. J. H. HU, *IEEE T. Ultrason. Ferr.* **50** (2003) 594.
13. M. D. HILL, G. S. WHITE and C. S. HWANG, *J. Am. Ceram. Soc.* **79** (1996) 1915.
14. A. FURUTA and K. UCHINO, *ibid.* **76** (1993) 1615.
15. Y. WANG, W. Y. CHU and L. J. QIAO, *Mater. Lett.* **57** (2003) 1156.



*Received 29 December 2004*
*and accepted 22 February 2005*